Pergamon

Journal of Structural Geology, Vol. 17, No. 8, pp. 1125 to 1137, 1995

0191-8141/95 $9.50+0.00

0191-8141(94)00129-4

The transpressional strain model applied to strike-slip, oblique-convergent and oblique-divergent deformation

R. W. KRANTZ

ARCO Exploration and Production Technology, Plano, TX 75075, U.S.A.

(*Received* 27 *September* 1993; *accepted in revised form* 2 *December* 1994)

Abstract—Zones of distributed shear deformation associated with strike-slip and oblique-convergent or oblique-divergent systems accommodate complex three-dimensional strains. Current models suggest that structural orientations within the zones depend on not only the magnitude of shear strain but also the degree of convergence or divergence. The transpressional strain model of Sanderson and Marchini is further developed here, and this study also focuses on relating structural orientations in map view to the magnitude of shear and the degree of convergence or divergence, and to the magnitudes of horizontal and vertical strains. Results include both the mathematical derivation and a set of nomograms relating the model parameters. Applications of the model to field examples and laboratory analogs show how the model can be used to determine the degree of convergence or divergence, and to calculate strain parameters. The model provides geologists with a method to evaluate and predict structural orientations, and to test map and cross-section interpretations.

INTRODUCTION

Strike-slip and oblique-convergent or oblique-divergent deformation commonly produce zones of distributed shear. Within these zones, smaller structures accommodate lateral translation of one zone boundary relative to the other. In strike-slip systems lacking a through-going fault, distributed shear accounts for all lateral displacement. In more mature systems, with one or more through-going strike-slip faults, adjacent sheared zones may still account for a significant portion of the overall lateral slip.

The simple strain ellipse model

Accepted models for strike-slip structural styles relate the coeval development and orientations of contractional, extensional, and strike-slip structures to horizontal simple shear (Sylvester 1988). Harding (1973, 1974) first described how these diverse structures correspond to a horizontal strain ellipse within a zone of simple shear (Fig. 1). In brief, the Harding model suggests that simple shear produces horizontal contractional and extensional incremental strains (principal horizontal strain axes) oriented at 45° to the shear. Thus a circular marker is deformed into an ellipse, inclined 45° to the direction of shear. The model predicts specific orientations for contractional, extensional and strike-slip structures according to the horizontal incremental strain ellipse.

The simple Harding-type model fails to address two important factors. The first concerns the change in finite strain orientations and structural geometries with progressive shearing. Most structures appear to rotate in the direction sympathetic to the overall shear. Second, few natural systems deform in ideal simple shear. Most contain a convergent or divergent component, producing oblique shear. Recent work (see below) suggests that

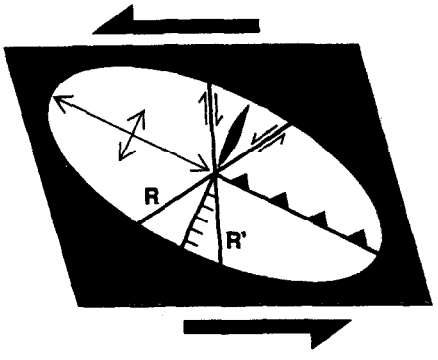

Fig. 1. Schematic map view of part of a distributed shear zone, showing the horizontal strain ellipse with long axis 'inclined' in the direction of shear. Compressional structures (folds, reverse faults) develop parallel to the long axis. Extensional structures (tension fractures, normal faults) develop parallel to the short axis. Conjugate strike-slip faults develop symmetrically about the short axis.

the orientations of both structures and horizontal strains depend on the degree of convergence or divergence. Thus the Harding-type model cannot predict structural orientations in the general case. Furthermore, the simple Harding-type model does not relate the magnitude of horizontal finite strains to either the amount of shear or the degree of convergence or divergence.

Other models

Further development of Harding's basic concept has lead to more sophisticated models. Crowell & Ramirez (1979) showed qualitatively how progressive shear relates to horizontal strain. They suggested that the finite strain ellipse rotates and elongates as shear increases, and that structural orientations reflect the rotation. Naylor *et al.* (1986) produced a series of strike-slip sand box experiments with a variable component of horizontal 'pre-load' across the strike-slip fault zone. They showed that initial orientations of conjugate en échelon

strike-slip faults depend on the degree of convergence or divergence. Neither of these models offered any quantitative relationships.

Several authors have quantitatively related structural geometries and strain orientations to the degree of convergence or divergence. Withjack & Jamison (1986) summarized the results of analog clay models and analytical stress–strain models for oblique rifting. Their models included the complete spectrum from extensional rifting to oblique-divergent rifting to strike-slip, and showed a predictable variation in fault type and orientation relative to the degree of obliquity. Much of their analysis focused on the initial formation of faults, and hence the relation to incremental strain, although they did briefly describe progressive deformation in some models. McCoss (1986) described an elegantly simple construction for solving the relative orientations of the incremental strain axes and the boundary displacement vector for zones of oblique-convergence or oblique-divergence. He also showed how the axes of the three-dimensional incremental strain ellipsoid vary in magnitude for the complete spectrum of deformation from contraction to strike-slip to extension. McCoss (1987) effectively demonstrated this spectrum with his annulus *or* 'ash-can lid' model.

Oblique deformation has also been studied in physical models. Tron & Brun (1991) reported on analog models of oblique rifting, and again included the spectrum of extension to oblique-divergence to strike-slip. They qualitatively related observed fault orientations to displacement vector but only briefly addressed progressive deformation. Smith & Durney (1992) described the development of dip-slip and strike-slip fault sets in clay models deformed in oblique-divergence. They very effectively related fault type and orientation and incremental strain state to the displacement vector orientation, as well as addressed three-dimensional strain issues and the degree of vertical thinning or thickening in a given model. Unlike the authors cited above, Richard *et al.* (1991) deformed analog models only in strike-slip. They did, however, qualitatively describe the rotations and overprinting of structures with progressive deformation and showed how fold axes became more parallel to the shear zone with increasing simple shear.

Mathematical models have addressed both the degree of obliquity and the relation of finite strain to progressive deformation. Sanderson & Marchini (1984) described the basic deformation matrix for three-dimensional transpression–transtension. Their model has formed the basis for several other investigations, including this one (see below for further discussion of the Sanderson and Marchini model). Fossen & Tikoff (1993) described a more general matrix for oblique deformation. Rather than applying pure shear, simple shear and volume change in some sequence, they showed how to model simultaneous pure and simple shear and dilation. Fossen & Tikoff (1993) showed quantitatively how finite strain orientations, magnitudes and rotations vary with progressive deformation. A subset of their more general model matched the Sanderson & Marchini (1984) model, but offered a more refined discussion of strain paths.

Jamison's (1991) model relates the obliquity of folds in domains bordering major strike-slip faults and the horizontal shortening accommodated by the folds to the degree of convergence. The model, however, is limited to systems of upright symmetric folds where no faults help to accommodate shortening. Although Jamison also described the relationship of convergent shear to horizontal extension, the model as presented does not apply the concept to fully describe two-dimensional and three-dimensional strains. Several of the applications discussed in this report use examples described by Jamison and compare results.

Purpose and content

Progress in understanding and predicting structural geometries in strike-slip systems depends on the development of quantitative models that relate geometric and kinematic parameters. This paper describes how the Sanderson & Marchini (1984) model can be further developed and focused on relating orientations and magnitudes of horizontal finite strains, amount of progressive shear, and the degree of convergence or divergence in zones of oblique shear. These parameters can be related mathematically or graphically, using a set of nomograms. The model accommodates the complete spectrum of deformation, from pure contraction to oblique-convergence to pure strike-slip to oblique-divergence to pure extension. The model also relates geometric and kinematic parameters for progressive deformation in shear zones. Although it describes three-dimensional strain, the model focuses on horizontal strains as revealed by geologic map patterns. This paper includes application of the model to field examples and laboratory analogs, and shows how the model can be used to determine degree of convergence or divergence, evaluate and predict structural orientations, and test map and cross-section interpretations.

THE TRANSPRESSIONAL STRAIN MODEL

As described by Sanderson & Marchini (1984) the model relates the three-dimensional strain of a domain undergoing distributed horizontal shear between two parallel vertical boundaries to the magnitude of shear and convergence (or divergence) of the boundaries (Fig. 2). The model assumes no volume change and no change in length parallel to the shear zone, so that convergence must be compensated by vertical thickening. The assumptions prohibit lateral escape of material.

Although few natural systems include parallel boundaries and ideally-distributed shear, the model can still be applied by defining appropriate domains.

The deformation matrix

Sanderson & Marchini (1984) define the deformation matrix

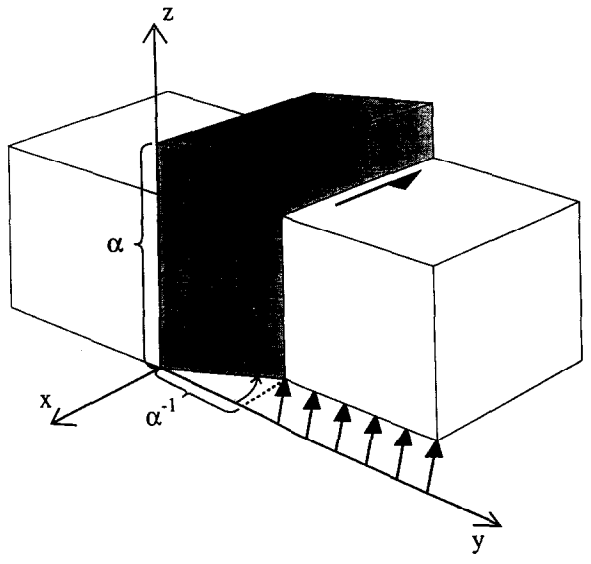

Fig. 2. Transpressional model and parameters. An original unit cube is transformed by a combination of distributed horizontal shear (ψ) parallel to the x-axis and convergence parallel to the y-axis. The deformed width is given by α^{-1}. After Sanderson & Marchini (1984).

$$\mathbf{D} = \begin{pmatrix} 1 & \alpha^{-1}\gamma & 0 \\ 0 & \alpha^{-1} & 0 \\ 0 & 0 & \alpha \end{pmatrix}, \quad (1)$$

where α^{-1} gives the convergence across the zone, parallel to the y-axis, α is the vertical thickening, parallel to the z-axis, and γ is the horizontal shear strain, parallel to the x-axis. (See Table 1 for a list of variables). Strictly speaking, α^{-1} is the ratio of the deformed width of the zone to the original width, and

$$\gamma = \tan\psi, \quad (2)$$

where ψ is the angular shear.

The deformation in the horizontal (x-y) plane can be described by

$$\mathbf{D} = \begin{pmatrix} 1 & \alpha^{-1}\gamma \\ 0 & \alpha^{-1} \end{pmatrix}. \quad (3)$$

The horizontal strain ellipse

In the undeformed state (x, y), a unit circle is described by

$$x^2 + y^2 = 1. \quad (4)$$

Table 1. Symbols and parameters used in the model derivation

$\mathbf{D}$	deformation matrix.
α^{-1}	stretch of unit square in y-direction (across shear zone).
α	stretch of unit square in z-direction (vertical).
γ	horizontal shear strain, parallel to x-direction.
ψ	angular shear.
ϕ	angle between long axis of horizontal strain ellipse and x-axis (shear direction).
S_{Hmax}	maximum horizontal stretch.
S_{Hmin}	minimum horizontal stretch.
S_T	transverse horizontal stretch, parallel to y-axis.
S_v	vertical stretch.
R	convergence ratio parameter.

In the deformed state (x', y'), the circle has been deformed into an ellipse given by

$$x'^2 - 2\gamma x'y' + (\alpha^2 + \gamma^2)y'^2 = 1. \quad (5)$$

The size and orientation of the ellipse can be described by S_{Hmax}, S_{Hmin} and ϕ (Fig. 3). S_{Hmax} is one-half the length of the major axis of the horizontal ellipse. S_{Hmin} is one-half the length of the minor axis, and ϕ is the orientation of the long axis, measured from the x-axis direction. Solving for these parameters in terms of α and γ (see Appendix 1) yields

$$\phi = \tfrac{1}{2}\arctan\left(\frac{2\gamma}{\alpha^2 + \gamma^2 - 1}\right), \quad (6)$$

$$S_{Hmax} = (1 - \gamma\tan\phi)^{-1/2}, \quad (7)$$

$$S_{Hmin} = (1 - \gamma\cot\phi)^{-1/2}. \quad (8)$$

These equations express the orientation (ϕ) of the horizontal strain ellipse and the magnitudes (S_{Hmax}, S_{Hmin}) of the horizontal principal stretch values.

The convergence factor: R

The degree of convergence or divergence can be expressed by the factor R, defined as the ratio of the component of convergence across the shear zone to the strike-slip component (Fig. 3). R is related to parameters of previously published models describing convergence or divergence as follows:

$R = \tan\beta$ (Sanderson & Marchini 1984),

$R = \tan A$ (McCoss 1986),

$R = \tan\alpha$ (Jamison 1991).

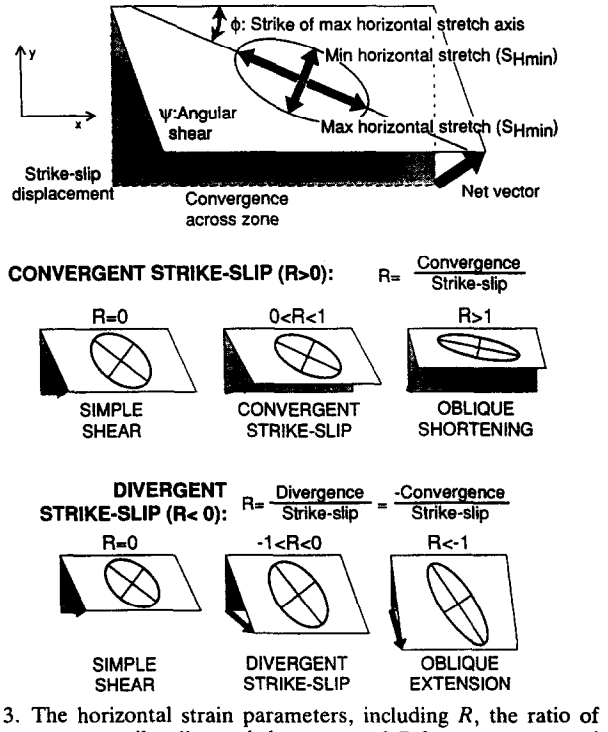

Fig. 3. The horizontal strain parameters, including R, the ratio of convergence to strike-slip, and the ranges of R for convergent and divergent shear.

Positive R values correspond to convergence; negative R values to divergence. For simple shear, R is zero. As the deformation approaches pure shortening, R approaches positive infinity. In between, R quantifies the components of oblique shortening. For $R < 1$, convergence dominates over strike-slip; for $R > 1$, strike-slip is dominant. Similarly, negative R values range from nearly zero to negative infinity, which corresponds to pure extension. R values less than or greater than -1 relate to dominant divergence or strike-slip, respectively.

Assuming that boundary displacement vectors remain constant, at least for some interval of deformation, R can approximate a deformation path. Thus determining R for a deformed oblique shear zone also determines the interrelationship of the horizontal strain parameters. (See Appendix 2 for the equations relating R to the other strain parameters.)

Transverse strain

Occasionally horizontal strain values other than the maximum or minimum principal strains may be available. Commonly seismic lines and geologic cross-sections are oriented perpendicular to the general structural trend, i.e. to the trend of the shear zone. Appendix 3 gives the stretch of a line perpendicular to the shear zone (in the deformed state) as

$$S_T = (\alpha^2 + \gamma^2)^{-1/2}. \quad (9)$$

Note that in general the transverse stretch, S_T, is not the same as the change in width of the shear zone, α^{-1}. The transverse stretch includes a component of shortening induced by the shear, γ. Only where $\gamma = 0$ (pure shortening or extension) does $S_T = \alpha^{-1}$.

Vertical strain

The vertical strain, expressed as stretch, is given by

$$S_V = \alpha = R\gamma + 1. \quad (10)$$

Summary

Using the equations given above (and in the appendices) it is possible to determine R, the ratio of the convergent component to the strike-slip component, α^{-1}, the change in width of the shear zone, and γ, the shear strain, from ϕ, the orientation of the horizontal strain ellipse (long axis) and any one of the horizontal stretch magnitudes: maximum, minimum, or transverse. Once R, α^{-1}, and γ have been determined, they can be used to calculate the other horizontal stretch magnitudes, and the vertical strain, thus specifying the complete three-dimensional deformation.

STRAIN PARAMETER NOMOGRAMS

Plotting the equations for the horizontal strain parameters yields a set of nomograms that relate the various model parameters. These nomograms can be used to determine strain values and to test map and cross-section interpretations (see Applications section).

Minimum horizontal stretch

The first nomogram relates ϕ, R and S_{Hmin}, the minimum horizontal stretch (Fig. 4). The nomogram plots S_{Hmin} on the horizontal axis and ϕ on the vertical axis. Each curve relates ϕ and S_{Hmin} for a constant R value, with progressive deformation increasing to the right. Thus the points along the vertical axis represent the initial orientation of the horizontal finite strain ellipse. Note that only the curve for simple shear ($R = 0$) starts at 45°. All curves for convergent shear ($R > 0$) start at lower angles, and all curves for divergent shear ($R < 0$) start at higher angles. As S_{Hmin} decreases (due to progressive deformation) each curve approaches the horizontal axis, suggesting a horizontal finite strain ellipse more and more nearly parallel to the shear zone. For convergent systems, the curves merge as S_{Hmin} approaches 0. For divergent deformation, each curve has an end point defined by the maximum values of γ, and hence minimum values of S_{Hmin}, allowed by each R value (see Appendix 2).

Figure 4 also shows how the nomogram relates the three parameters for a specific example. In this example, the horizontal strain ellipse trends at 20° to the shear zone ($\phi = 20°$), with a $S_{Hmin} = 0.5$. On the nomogram, these values intersect on the curve for $R = 0.5$, indicating a convergent system with half as much convergence as strike-slip (or twice as much strike-slip as convergence).

Maximum horizontal stretch

The second nomogram (Fig. 5) relates ϕ, R and S_{Hmax}, the maximum horizontal stretch. Similar to the

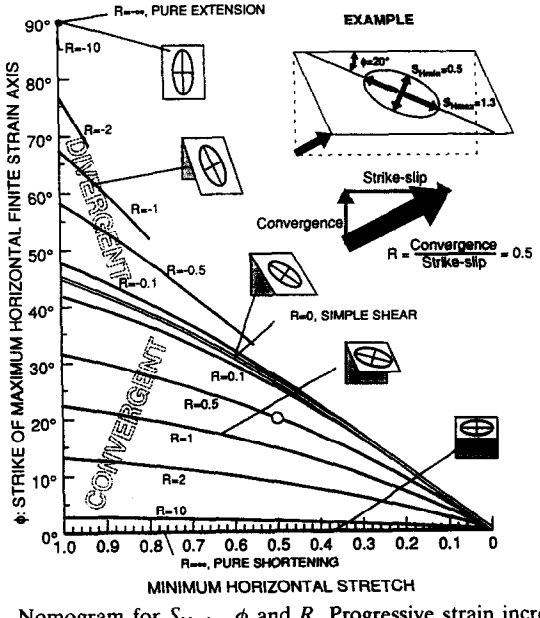

Fig. 4. Nomogram for S_{Hmin}, ϕ and R. Progressive strain increases from left to right. The white dot plots the correct location for the example shown in the upper right.

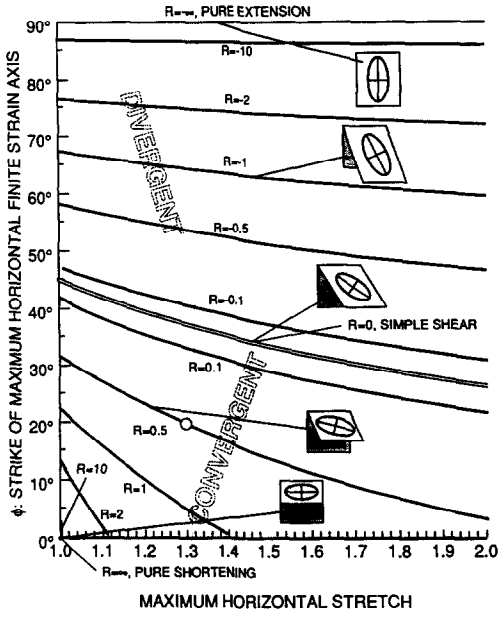

Fig. 5. Nomogram for S_{Hmax}, ϕ and R. Progressive strain increases from left to right. The white dot corresponds to the example shown in Fig. 4.

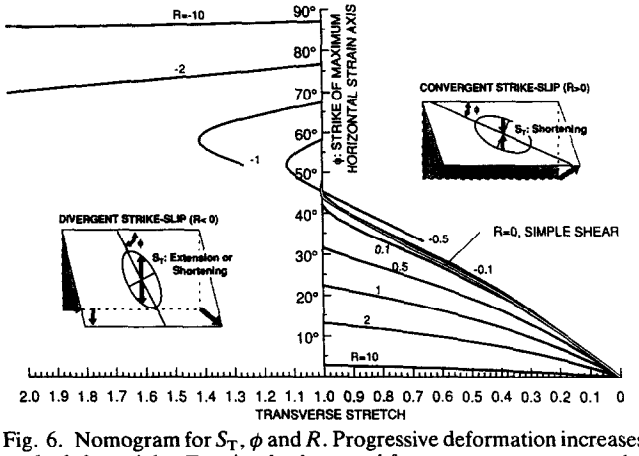

Fig. 6. Nomogram for S_T, ϕ and R. Progressive deformation increases to the left or right. For simple shear and for convergent systems, the transverse stretch is always a shortening. For divergent systems, the curves are more complex. See text for details.

first graph, this nomogram plots S_{Hmax} along the horizontal axis and ϕ along the vertical axis. Each curve relates these two parameters for a given R value, with progressive deformation increasing to the right. Once again, points along the vertical axis reveal the initial orientation of the horizontal finite strain ellipse, with $R = 0$ at 45°. With progressive deformation, S_{Hmax} increases and ϕ decreases for all values of R. The curves do not converge on this plot because S_{Hmax} ranges from one to infinity, and only a limited portion of that range is shown in Fig. 5.

Figure 5 also shows how this nomogram relates the three parameters for the same example as in Fig. 4. Taking $\phi = 20°$ and R = 0.5, the nomogram predicts $S_{Hmax} = 1.3$. Thus by measuring one horizontal principal stretch (minimum) and the orientation of the horizontal strain ellipse, and determining the R value, it is possible to predict the other horizontal principal stretch (maximum).

Transverse stretch

The relationship of transverse stretch to the other parameters is more complex (Fig. 6). The transverse stretch is not the same as the convergence or divergence across the shear zone, but includes a component of shortening induced by the shear. For convergent systems, the transverse stretch is always a shortening ($S_T < 1.0$). For divergent systems, the transverse strain may be a shortening ($S_T < 1.0$) or an extension ($S_T > 1.0$), depending on the value of R and the magnitude of shear strain.

Figure 6 shows the nomogram for transverse strain. As in the other nomograms. S_T plots along the horizontal axis, with transverse stretch decreasing to the right and increasing to the left. The vertical axis again shows ϕ, the orientation of the horizontal finite strain ellipse (long axis). The curve for simple shear ($R = 0$) starts at $\phi = 45°$ and decreases to zero as S_t decreases. The curves for convergent systems ($R > 0$) start at lower initial angles and also converge on zero. The curves for divergent systems ($R < 0$) show more complex patterns. For strongly divergent systems ($R \leq -2$), the curves start at high initial ϕ angles and decrease to the left, with increasing transverse stretch. For moderately to slightly divergent systems ($-1 \leq R \leq -0.1$), the curves initially head to the left (increasing transverse stretch) but then head to the right (decreasing transverse stretch). For some R values (e.g. $R = -0.5$) the curve enters the transverse shortening field. Thus for slightly divergent systems, the transverse stretch, although initially an extension, ultimately becomes a shortening.

Shear strain

The final nomogram (Fig. 7) relates the horizontal shear strain, γ, to R and ϕ. The shear strain is the tangent of the angular shear, and plots along the horizontal axis. Like the other nomograms, ϕ plots along the vertical axis. The curves for different R values again initiate at the vertical axis and head to the right with progressive shear. For pure strike-slip and convergent systems ($R \geq 0$), the curves merge as γ approaches infinity. For divergent systems ($R < 0$), the curves end at maximum γ values, given by equation (A18).

Summary

Figure 8 summarizes the variation in shape and orientation of the horizontal finite strain ellipse, as well as the horizontal stretch parameters, for a range of R values. Each row represents progressive deformation with a constant R value, i.e. constant boundary displacement vector. Shear strain, γ, increases to the right. Each example shows the deformed shapes of the original square and circle; all ellipses are drawn to scale. Each example also gives the magnitudes of ϕ, S_{Hmin}, S_{Hmax} and S_T.

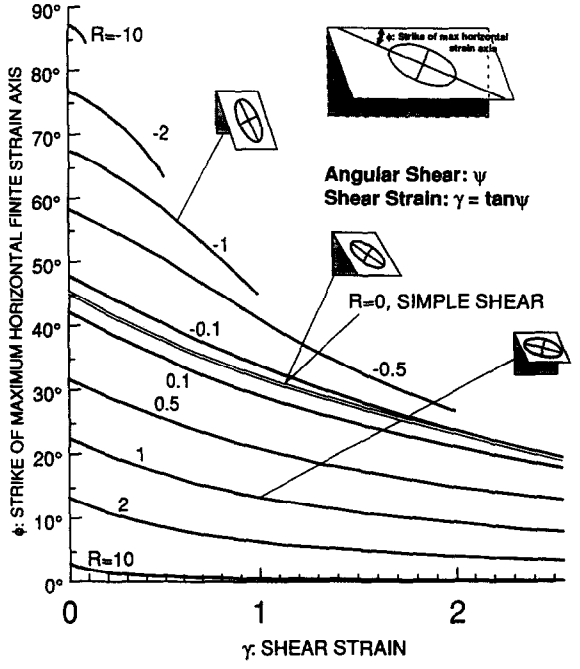

Fig. 7. Nomogram for the shear strain parameters. Progressive shear increases to the right.

For simple shear ($R = 0$), horizontal surface area remains constant so the area inside the ellipse also remains constant. As γ increases, the aspect ratio of the ellipse increases and ϕ decreases so the ellipse becomes closer to parallelism with the shear direction. The magnitudes of both horizontal finite strains also increase, so that even moderate amounts of shear strain ($\gamma \geq 0.5$) involve large horizontal shortening and extensional strains. Thus distributed shear in a pure strike-slip setting should produce both compressional and extensional structures.

For convergent shear ($R > 0$), surface area decreases and the ellipse shrinks. Assuming no volume change, the model predicts vertical thickening. The ellipse does rotate with progressive shear strain, as with pure-slip, but initiates at lower ϕ angles. Note that for strongly convergent systems ($R \geq 2$), minimum horizontal stretch decreases rapidly but maximum horizontal stretch grows very slowly. These systems should be dominated by compressional structures that also accommodate vertical thickening.

Finally, for divergent shear ($R < 0$), surface area and the ellipse both grow. Again given no volume change, the model predicts vertical thinning. The ellipse initiates at higher angles but still rotates towards the shear direction. The maximum horizontal stretch grows much more rapidly than the minimum horizontal stretch decreases, suggesting that extensional structures should dominate. Note that divergent systems reach a maximum shear strain value, determined by R.

APPLICATIONS

The transpressional strain model can be used to determine convergence ratios, predict horizontal strain parameters and test interpretations. The model can even be used to 'balance' strains in three dimensions. The applications discussed below come from both field and experimental model examples of distributed shear systems.

In addition to the assumptions already given for the model itself (constant volume, no change in length parallel to the shear direction and homogeneous distributed shear), these applications make one more fundamental assumption: that the orientations of structures observed accurately reflect the orientation of the horizontal finite strain ellipse. That is, folds and reverse faults trend parallel to the long axis, tensional fractures and normal faults trend parallel to the short axis, and primary en échelon strike-slip faults develop in conjugate pairs, with the acute angle bisected by the short axis. Clearly this assumption overlooks the fact that structures initiate at an angle corresponding to the incremental strain field and are then modified by progressive deformation. As discussed in the example of experimental folds below, the modification need not be a simple passive rotation. Most systems also contain structures developed at different stages, including a mix of incremental and finite strain features.

None of the examples completely satisfies the assumptions. Most involve discontinuous deformation, at some scale of observation, and none have parallel bounding faults. On the regional scale considered, however, shear is distributed among smaller structures. Furthermore, structural orientations are consistent over at least the domain considered. For the examples shown, the shear direction is assumed to trend parallel to through-going strike-slip faults, if present, or to the regional trend of the zone of en échelon structures. Although not ideal, the examples allow at least a first-order approximation of the convergence ratios and the strain magnitudes involved.

Finally, the accuracy of the model depends on measuring parameters that show natural variation in the field. Structural orientations commonly vary by at least $\pm 10°$. Strain calculations commonly have errors of $\pm 20\%$ or more. The issue of progressive deformation also introduces a variable error, depending on the degree of passive rotation. Thus the nomograms and equations cannot yield precision better than $\pm 20\%$ for α and γ, or determine R to better than one significant figure. The uncertainty in R means that the model may be used to resolve systems with various degrees of convergence or divergence (see Table 2).

Determining strain magnitudes

The first examples demonstrate how the model can make use of one or more known strain parameters to determine the others. In each case, ϕ, the orientation of the horizontal strain ellipse, is determined from map patterns of folds or faults. Horizontal finite strain magnitudes, determined from cross-sections or field measurements, provide the other constraint. In some examples

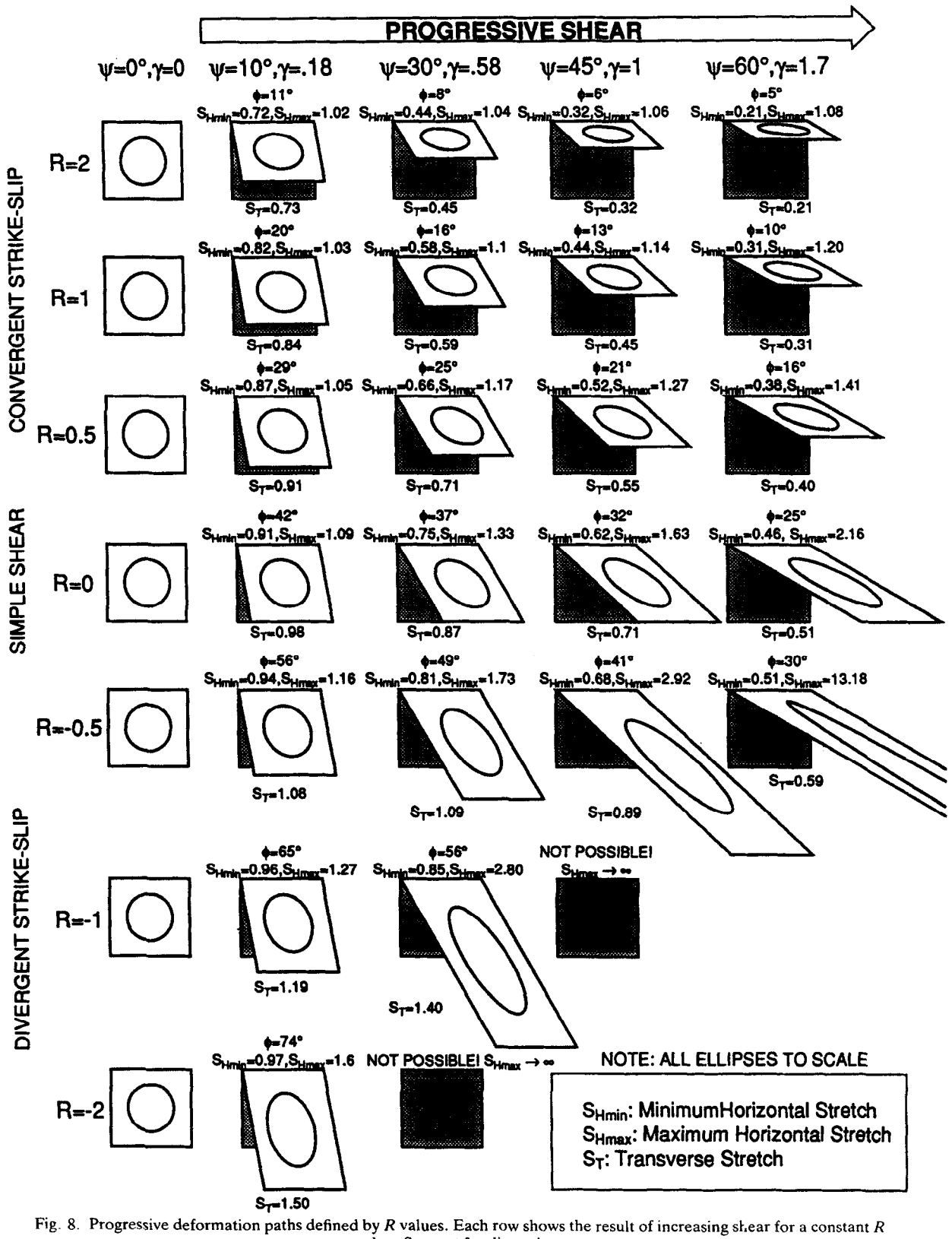

Fig. 8. Progressive deformation paths defined by R values. Each row shows the result of increasing shear for a constant R value. See text for discussion.

the magnitude of strike-slip offset accommodated by the shear can also be calculated.

Figure 9 is a geologic map of part of the Durmid Hills, along the San Andreas fault in southern California (Babcock 1974). Folds trend obliquely to the San Andreas fault. Taking the average fold trend as the long axis of the horizontal strain ellipse yields a value for ϕ of 30°. Burgmann (1989, 1991) measured horizontal strains in a boudinaged ash bed in the same region. He determined a maximum horizontal stretch of 1.63 ± 0.05 parallel to the fold trend. On the nomogram for S_{Hmax} (Fig. 5) these two parameters define an R value of 0.05, nearly pure strike-slip but slightly convergent (see Table 2). Jamison (1991) determined a convergence angle (his α) of 5–10° for this region, equivalent to an R value of 0.1–0.2.

Table 2. Resolving degrees of convergence of divergence and ranges of R

Nearly pure shortening	$R > 10$
Strongly convergent	$2 < R < 10$
Moderately convergent	$0.5 < R < 2$
Slightly convergent	$0.1 < R < 0.5$
Nearly pure strike-slip	$-0.1 < R < 0.1$
Slightly divergent	$-0.5 < R < -0.1$
Moderately divergent	$-2 < R < -0.5$
Strongly divergent	$-10 < R < -2$
Nearly pure extension	$R < -10$

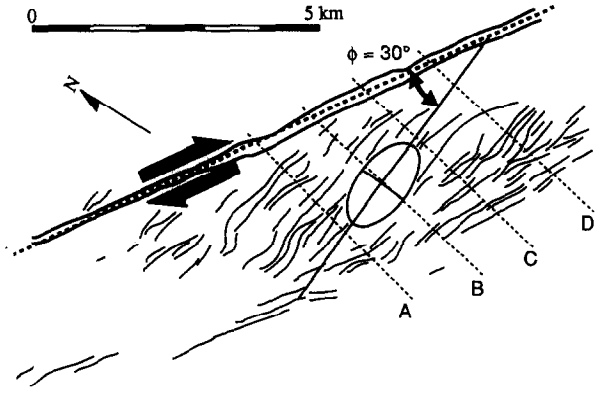

Fig. 9. Surface traces of folds along the San Andreas fault in the Durmid Hills, southern California (after Babcock 1974). The average fold trend defines the long axis of the horizontal finite strain ellipse, and ϕ = 30°. Burgmann (1989, 1991) measured average horizontal extension of 63% parallel to the fold axes. A through D indicate the positions of cross-sections discussed in the text.

This R value, along with ϕ, can now be used to determine the other strain parameters (Table 3). The nomogram for S_{Hmin} (Fig. 4) predicts a horizontal stretch of 0.59. This value agrees well with the 40–50% shortening determined by Babcock (1974) from cross-sections. Thus the cross-sections, if not precisely correct, at least contain the correct amount of shortening. The transverse stretch nomogram (Fig. 6) predicts a transverse stretch of 0.67. Thus transverse cross-sections should show less shortening than those drawn perpendicular to the folds. The model predicts significant transverse shortening even though the zone deformed by nearly ideal simple shear (i.e. very little convergence). The shear strain nomogram (Fig. 7) predicts a value of 1.1 for γ, equivalent to an angular shear of 48°. Taking the width of the folded domain as the final width of the shear zone, about 4 km, this shear strain value suggests that the folding accommodated about 4.4 km of lateral displacement. Thus any determination of the total offset in the Durmid Hills must add 4.4 km to slip determined for the San Andreas fault proper. The values of R and γ predict a vertical stretch of 1.06, suggesting a slight vertical thickening within the shear zone.

Figure 10 shows a series of three strike-slip sand box models completed at ARCO. From top to bottom, they show the final map pattern of en échelon faults developed in simple shear, convergent shear and divergent shear. All three experiments used a fine-grained garnet sand with an angle of internal friction of 22°. Offset of markers on the surface determined the magnitude of strike-slip as well as the width of the shear zone at the surface. Thus with known R values, the fault orientations (and ϕ angle) can be used to predict shear strains (Table 3).

For the simple shear experiment, R = 0, the faults strike 27° from the shear direction. Assuming these faults are the synthetic half of a conjugate pair, the short

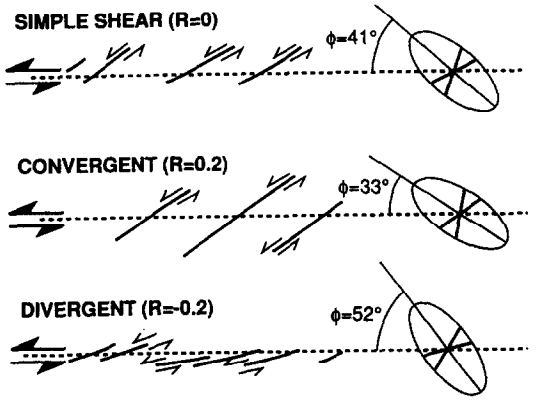

Fig. 10. Fault patterns produced in sandbox models deformed in simple shear, convergent strike-slip and divergent strike-slip. The dashed line shows the position of the fault in the 'basement' underlying the sand pack.

Table 3. Strain parameters for examples in text. Known or assumed values given in **bold type**

Example and interpretation #	ϕ Angle	R	tan α_j*	S_{Hmin}	S_{Hmax}	S_T	γ	Comments
Durmid Hills, California	**30°**	0.05	0.1–0.2	0.59	**1.63**	0.67	1.1	Agrees with Jamison (1991)
Experimental faults (simple shear)	**41°**	**0**		0.92	1.07	0.99	0.15	
Experimental faults (convergent)	**33°**	**0.2**		0.85	1.09	0.93	0.25	
Experimental faults (divergent)	**53°**	**−0.2**		0.95	1.10	1.02	0.13	
Trinidad	**24°**	0.6	0.6	0.58	1.08	**0.79**	0.33	Agrees with Jamison (1991)
Experimental folds	**20°**	**0**	0	0.36	2.73	0.39	2.4	
Eagle Canyon Fault, int.1	**22°**	**0**		0.40	2.57	0.43	2.1	Strain values too high
Eagle Canyon Fault, int. 2	**22°**	0.8		**0.75**	1.07	0.78	0.31	Better fit of strain values
Nacimiento Uplift, int. 1	**20°**	**0.1**		0.38	2.16	0.40	2.2	Strain values too high
Nacimiento Uplift, int. 2	**20°**	**1**		0.81	1.04	0.83	0.2	Better fit of strain values
Lake Basin, normal fault int.	**35°**	0.3		0.94	1.04	0.97	**0.1**	Reasonable strain values
Lake basin, strike-slip int.	**5°**	4.6		0.68	1.004	0.68	**0.1**	Too much shortening
Rinconada Fault	**18°**	1	1.2	0.68	1.07	0.70	0.38	Reasonable strain values
Andaman Sea, int. 1	**32°**	?		?	?	**1.13**	?	Parameters undefined
Andaman Sea, int. 2	**32°**	0.3		0.78	**1.15**	0.86	0.4	Transverse shortening?
Andaman Sea, int. 3	**32°**	**0**		0.62	1.61	0.71	1	Incompatible results

*α_j is the convergence vector defined by Jamison (1991). Tan α_j is equivalent to R.

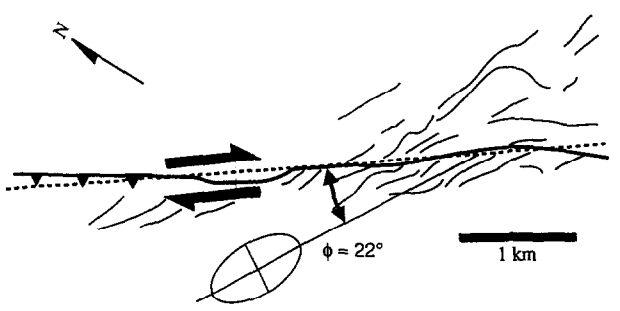

Fig. 11. Surface traces of folds along the Eagle Canyon fault, Mecca Hills, southern California, after Harding *et al.* (1985). The oblique folds along the southeast portion of the mapped fault define a ϕ angle of 22°. Strain magnitudes are unknown.

axis of the horizontal finite strain ellipse strikes 27° + 22° = 49° from the shear direction. The observed long axis strike, ϕ, is thus 41°. On the shear strain nomogram (Fig. 7), these values for R and ϕ predict a shear strain of 0.15. Comparing the width and offset across the shear zone suggests a measured γ value of 0.12. For the convergent experiment, $R = 0.2$, the observed fault strike is 35° and $\phi = 33°$. The value predicted for γ is 0.25, compared to a measured value of 0.20. For the divergent experiment, $R = -0.2$, the observed fault strike is 15° and $\phi = 53°$. The value predicted for γ is 0.13, compared to a measured value of 0.13. Thus the model does a good job of predicting the shear strain magnitudes based on fault orientations.

Jamison (1991) analyzed the structural patterns of Trinidad (Kugler 1959). Reverse faults and folds trend oblique to the El Pilar fault, defining a value for ϕ of 24°. Kugler's (1959) cross-section trends north–south, perpendicular to the fault and shear direction. The central part of the cross-section reveals 21% horizontal shortening ($S_T = 0.79$). Using the transverse stretch nomogram (Fig. 6), these values define $R = 0.6$ (moderately convergent) (Table 3). The convergence angle determined by Jamison (1991), 30°, also yields an R value of 0.6.

The values determined for R and ϕ from Trinidad predict $S_{Hmin} = 0.76$ and $S_{Hmax} = 1.08$. These values seem reasonable based on the map patterns; strike-slip and normal faults as mapped could easily accommodate 8% extension parallel to the fold axes and reverse faults. The model also predicts $\gamma = 0.33$, so that the portion of the distributed shear zone exposed on the island, about 60 km wide, accommodated about 20 km of lateral displacement. The value of R suggests a moderately convergent system, with a ratio of strike-slip to convergence of about 1.7.

Odonne & Vialon (1983) deformed layered sequences of wax in simple shear. By definition, $R = 0$. The average trend of the fold crests determines a ϕ value of 20°. On the nomograms, these values can be used to determine the other strain parameters (Table 3). The shear strain nomogram (Fig. 7) predicts a γ value of 2.4, equivalent to an angular shear of 67°. Dividing the width of the sheared zone, 20 cm, by the total offset, 51.5 cm, reveals an observed value of γ of 2.6, equivalent to an angular shear of 69°. The other nomograms also predict that $S_{Hmax} = 1.73$, $S_{Hmin} = 0.36$ and $S_t = 0.39$ (shortening). Odonne & Vialon (1983) do not provide quantitative estimates of horizontal strain, but the schematic cross-section they show seems compatible with the horizontal shortening estimate. As for the large horizontal extension predicted, they point out that the wax used accommodates a large amount of stretching and thinning before rupturing.

Using the same data from Odonne & Vialon (1983), Jamison (1991) determined a value for γ of only 1.3. The difference in shear strain magnitude compared to this analysis may result from the interpretation of structural geometries inherent in the two models. The transpressional strain model assumes that structures, such as folds, accurately reflect the cumulative strain rate, and that geometries correspond to finite strain axis orientations. Jamison's model assumes that folds form at some initial angle and then rotate passively and tighten with progressive shear. Odonne and Vialon also suggest that fold axes originate at 45° to the shear direction (for simple shear), and rotate passively as folds tighten. Using the transformation equations of the transpressional model, a linear element originally at 45° and subjected to a shear strain of 2.6 (observed value) will have a final orientation of 15°. This value differs enough from the observed $\phi = 20°$ to suggest that the folds do not rotate passively. The folds must evolve through a refolding and rotational process that more accurately reflects the accumulated strain.

Making strain parameter estimates

In many cases, all horizontal strain parameters remain unknown. Only ϕ, the orientation of the horizontal strain ellipse relative to the shear direction, can be determined. Even in such cases, the model can be used to constrain the strain parameters to reasonable estimates, based on map patterns and tectonic setting.

Figure 11 shows a segment of the Eagle Canyon fault, a splay of the San Andreas fault in the Mecca Hills, southern California (Harding *et al.* 1985). The oblique trend of the folds defines a ϕ value of 22°, measured relative to the through-going fault. Unfortunately, no horizontal strain values have been published. The model can still be applied by making an estimate for one parameter and determining the others. This process is continued until reasonable values emerge for all parameters.

The first attempt assumes that $R = 0$. This may be a reasonable assumption for a short splay off a major strike-slip fault. The nomograms, however, suggest otherwise (Table 3). Using $R = 0$ and $\phi = 22°$, the model predicts that $S_{Hmin} = 0.40$, $S_{Hmax} = 2.57$ and $S_t = 0.43$. The value of γ, 2.1, implies a large amount of distributed shear. These strain magnitudes seem much too high for the structural geometries shown on the map, especially the large horizontal extension, since the map shows few normal faults or other extensional structures.

The second attempt assumes that $S_{Hmax} = 1.10$. This value allows for minor extension parallel to the fold axes. The nomograms now suggest that $R = 0.8$, $S_{Hmin} =$

0.75, $S_t = 0.78$ and $\gamma = 0.3$. All the strain parameters are now compatible with the map. The R value suggests a moderately convergent distributed shear, with nearly equal convergence and strike slip. Even if the strain magnitude estimates are incorrect by 10–20%, the model supports a convergent strike-slip interpretation. Note that as mapped by Harding *et al.* (1985) the Eagle Canyon fault displays a significant reverse separation to the northwest of the folded domain.

Chapin & Cather (1983) analyzed the western margin of the Nacimiento Uplift (Baltz 1967). They interpreted the oblique folds and faults there as the result of very slightly convergent strike-slip displacement (and uplift) along the margin. The first attempt at applying the model thus assumes $R = 0.1$ (Table 3). The oblique folds define $\phi = 20°$. The nomograms suggest that $S_{Hmin} = 0.38$, $S_{Hmax} = 2.16$, $S_t = 0.40$ and $\gamma = 2.2$. All of these strain magnitude estimates seem much too high, especially the maximum horizontal extension value, relative to the map pattern and the relative lack of normal faults or other extensional structures.

The low ϕ angle suggests a moderately convergent shear interpretation. Assuming $R = 1$, the model predicts more reasonable strain parameters. The nomograms show that $S_{Hmin} = 0.81$, $S_{Hmax} = 1.04$, $S_t = 0.83$ and $\gamma = 0.2$. All of these values better fit with the map, especially the small maximum horizontal stretch. Again, even with the potential error in horizontal strain estimates, the likely value for R is significantly greater than zero, which supports a more strongly convergent interpretation for the Nacimiento Uplift margin than proposed by Chapin & Cather (1983). Better horizontal strain estimates would improve the resolution and confidence of the model application.

Determining fault types

Another application of the model, potentially useful in subsurface work, involves faults with unknown displacements. Figure 12 shows the Lake Basin fault zone of Montana, as interpreted by Harding *et al.* (1985) after mapping by Alpha & Fanshawe (1954) and Smith (1965). The map shows a zone of an échelon faults arranged in a linear zone, but with unknown displacements. Harding *et al.* (1985) interpreted these faults as en échelon normal faults. If true, then the long axis of the horizontal finite strain ellipse trends perpendicular to the faults and $\phi = 35°$ (Fig. 12). Because no throughgoing fault exists at the surface, the total shear strain must be small. For $\gamma = 0.1$ and $\phi = 35°$, the shear strain nomogram suggests that $R = 0.3$ (Table 3). Using this R value, the other nomograms predict $S_{Hmin} = 0.94$, $S_{Hmax} = 1.04$ and $S_t = 0.97$.

Alternatively, the en échelon faults may be interpreted as synthetic ('R') strike-slip faults, one of the two conjugate strike-slip fault sets. If true, and assuming that each conjugate set strikes at 30° from the maximum horizontal shortening direction, the horizontal strain ellipse would trend nearly parallel to the zone and $\phi = 5°$ (Fig. 12). Assuming again that $\gamma = 0.1$, the nomograms

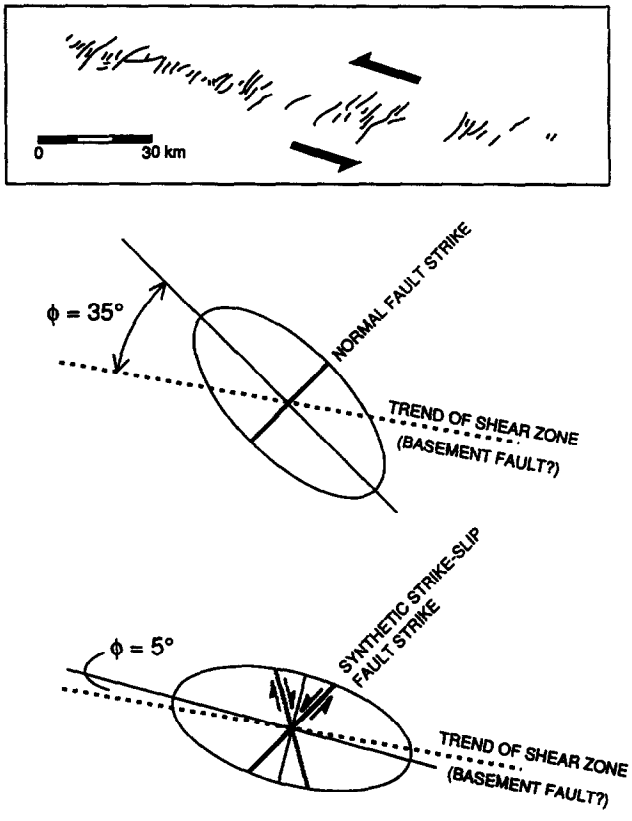

Fig. 12. Map and alternate interpretations for the Lake Basin fault zone, Montana. The map after Harding *et al.* (1985) shows en échelon faults with unknown displacement. The normal-slip interpretation yields $\phi = 35°$. The strike-slip interpretation yields $\phi = 5°$.

predict that $R = 4.6$, $S_{Hmin} = 0.68$, $S_{Hmax} = 1.004$ and $S_t = 0.68$ (Table 3).

Comparing the two alternatives, the normal fault interpretation seems more reasonable. All horizontal strain magnitudes are small, as might be expected with short, minor faults. The smaller R value suggests slightly convergent strike-slip, compatible with mostly lateral displacement on a basement fault zone. In contrast, the strike-slip fault interpretation requires large horizontal shortening strains, and suggests a large R value indicating dominant convergence. Such convergence may be difficult to reconcile with structures at deeper levels.

Three-dimensional strain analysis

Strain estimates derived from the model, coupled with data on the size of the shear domain, can fully constrain the three-dimensional deformation. Precision depends on the accuracy of the strain parameters used, but even where these are only estimates, the model can yield important first-order results.

Diblee (1976) mapped folds in the Monterey Formation along part of the Rinconada fault in southern California. The oblique fold trend defines $\phi = 18°$. Making estimates and testing results, as demonstrated above, the model suggests that $R = 1$ provides reasonable results (Table 3: $S_{Hmin} = 0.68$, $S_{Hmax} = 1.07$, $S_t = 0.70$ and $\gamma = 0.38$). R values much lower than this require very large horizontal strains. Solving equation (A17) for α and substituting the values for R and γ yields

$\alpha = 1.38$ and $\alpha^{-1} = 0.72$. The results of Jamison's (1991) analysis for the folds along the Rinconada fault determined a convergence angle of 50°, equivalent to a value for R of 1.2. He also determined a maximum horizontal shortening of 7–14% (minimum horizontal stretch of 0.86–0.93), based on fold limb dips. Although his horizontal shortening estimate seems low, the degree of convergence matches closely that determined here.

The deformed width of the folded domain is about 12 km. Since α^{-1} is defined as the deformed width divided by the original width, then the original width of the folded domain was about 17 km, suggesting 5 km of convergence across the shear zone. With $R = 1$, the strike-slip component is also 5 km. Note that this strike-slip displacement is distributed on either side of the Rinconada fault and does not include offset on the fault itself. The vertical strain (thickening) is given by α. Whatever the original thickness of material involved in the distributed shear, the final thickness is greater by 38% (not corrected for erosion), which matches the positive topographic relief.

Evaluating geologic interpretations

The model has its greatest potential in evaluating geologic interpretations. By comparing strain parameters and geometries, the model can identify which interpretations are allowed by the data and which are not.

Harding (1985) mapped an extensive system of parallel normal faults adjacent to a major strike-slip fault in the Andaman Sea. The average fault strike yields a ϕ value of 32°. Harding (1985) also showed a cross-section interpreted along a seismic line nearly normal to the strike-slip fault. Restoring bed lengths from the cross-section reveals an extensional strain of 13%. Although not truly perpendicular to the shear direction (through-going fault), the cross-section approximates the transverse stretch. Table 3 gives the results for the values $\phi = 32°$ and $S_T = 1.13$. Note that this transverse stretch plots on an undefined region of the nomogram (Figure 6). These values also do not yield numerical results from the model equations. Essentially, transverse stretch > 1 is not predicted for ϕ values less than 45°.

Assuming $S_{Hmax} = 1.15$, the nomograms and equations now yield coherent results (Table 3). Although values of $R = 0.3$ and $\gamma = 0.4$ seem reasonable, $S_{Hmin} = 0.78$ and $S_T = 0.86$ (shortening) do not agree with the map or cross-section interpretations. Instead, by assuming $R = 0$, the nomograms yield values of $\gamma = 1$, $S_{Hmin} = 0.62$, $S_{Hmax} = 1.61$ and $S_T = 0.71$ (shortening). Again, these values do not fit with the map or cross-section interpretations as shown. Other assumed values for R result in even worse fits.

The discrepancy can be resolved in several ways. First, the model may not be appropriate for the Andaman Sea system. One or more assumptions may be violated. For example, the deformed zone may accommodate distributed extension parallel to the shear direction. This extension might produce a lower apparent ϕ angle. Second, either the map or cross-section may be wrong. Assuming the map is based on parallel seismic sections, the correlations of faults and thus their apparent strike orientations may be incorrect. In both map and cross-section view, structures accommodating significant horizontal shortening may not be recognized. Third, the normal faults and the strike-slip faults may not be coeval products of the same deformation. If the normal faults predate the strike-slip fault, then their relative orientations have no direct relationship. In any case, the structures cannot be explained by the simple shear model as proposed by Harding (1985).

DISCUSSION AND CONCLUSIONS

The transpressional strain model and applications described above have implications for both basic geometric/kinematic relationships and practical interpretation. These implications hold for the complete spectrum of oblique-convergent to simple shear to oblique-divergent systems.

Implications for relating geometries and strain

(1) The initial orientation of the horizontal finite strain ellipse (i.e. after the first increment of strain) depends entirely on the ratio of convergence or divergence to strike-slip. Strongly convergent shear produces an ellipse nearly parallel to the shear direction. Simple shear produces a strain ellipse at 45° (but only for the initial increment). Divergent shear produces initial strain ellipse orientations at high angles to the shear direction.

(2) The orientation of the horizontal finite strain ellipse in the final state depends on both the ratio of convergence to strike-slip and on the magnitude of shear. With increasing shear, strain ellipses for all types of systems become more nearly parallel to the shear direction.

(3) Each specific combination of finite strain ellipse orientation and convergence ratio implies a specific set of horizontal strain values. The differences in maximum horizontal stretch, minimum horizontal stretch, transverse stretch, and shear strain can be used to distinguish shear systems that have the same apparent ellipse orientations but different convergence ratios.

(4) The transverse stretch, i.e. what is revealed in a cross-section perpendicular to the shear zone, is not the same as the convergence or divergence of the boundaries. The transverse stretch contains a component of shortening induced by the shear, in addition to the convergence. Thus even systems without convergence (ideal simple shear) will show shortening in transverse cross-sections.

Practical implications

(1) Where at least one strain parameter is known, the model can solve for the others. Thus by measuring maximum horizontal stretch, for example, the model

provides minimum horizontal stretch, transverse stretch, shear strain and vertical stretch.

(2) Where only the orientation of the horizontal finite strain ellipse is known, the model can estimate the reasonable range of the other parameters and constrain the possible deformational setting (i.e. strike-slip that is strongly or slightly convergent or divergent).

(3) Specifying horizontal strain values or ranges allows testing of cross-section and map interpretations. For example, do cross-sections reveal the correct magnitudes of shortening or extension? Do maps show the required proportion of compressional and extensional structures?

(4) Where the width of the shear zone is known, the value of shear strain provided by the model allows for the calculation of the amount of lateral offset accommodated by distributed shear. This offset must be added to displacement on through-going faults to determine the total offset for a strike-slip system.

General conclusions

Structural geometries in zones of distributed shear depend not only on the magnitudes of horizontal shear but also on the ratio of convergence or divergence. The transpressional strain model effectively relates the geometric and kinematic parameters for distributed shear deformation, and constrains the possible interpretations for a given system. Specifying the convergence/divergence ratio and one strain parameter strictly defines the others.

In general, systems without significant convergence or divergence (near simple shear) develop structures corresponding to an initial strain ellipse oriented at about 45° to the shear direction. With increasing horizontal shear, the finite strain ellipse trends at lower angles, but both the maximum horizontal stretch and the minimum horizontal stretch change rapidly. Thus compressional and extensional structures should develop about equally. Even without significant convergence, systems deformed under pure strike-slip conditions develop large transverse shortening strains with increasing shear.

Moderately to strongly convergent systems develop structures corresponding to a horizontal finite strain ellipse at low angles to the shear direction. Minimum horizontal stretch and transverse stretch decrease rapidly with increasing shear, but maximum horizontal stretch grows more slowly to a limited value. These systems should be dominated by compressional structures. In contrast, moderately to strongly divergent systems should be dominated by extensional structures corresponding to finite strain ellipses at higher angles to the shear direction. Maximum horizontal stretch grows rapidly while minimum horizontal stretch is limited. Transverse stretch may reveal extension or shortening depending on divergence ratios. Finally, determining the ratio of convergence or divergence for a system allows for evaluation of the geologic interpretation, both in terms of near-surface geometries and allowable geometries at depth.

Acknowledgements—Kris Meisling, Van Mount, Bill Kilsdonk, Bill Hill and Russell Davies provided helpful reviews of this and earlier versions of the manuscript. David Sanderson, Basil Tikoff and Peter Hudleston provided critical reviews and editorial improvements. Cristina Hart helped prepare the final manuscript. I thank ARCO Exploration and Production Technology for permission to publish this paper.

REFERENCES

Alpha, A. G. & Fanshawe, J. R. 1954. Tectonics of northern Bighorn basin area and adjacent south-central Montana. Billings Geological Society Guidebook, 5th Annual Field Conference, 72–79.

Babcock, E. A. 1974. Geology of the northeast margin of the Salton Sea Trough, Salton Sea, California. *Bull. geol. Soc. Am.* **85**, 321–332.

Baltz, E. H. 1967. Stratigraphy and regional tectonic implications of part of Upper Cretaceous and Tertiary rocks, east–central San Juan basin. New Mexico. *Prof. Pap. U.S. geol. Surv.* **552**.

Burgmann, R. 1989. Transpressional strain along the southern San Andreas fault, Durmid Hills, California (abstract). *Geol. Soc. Am. Abs. Prog.* **21**, A264–A265.

Burgmann, R. 1991. Transpression along the southern San Andreas fault, Durmid Hill, California. *Tectonics* **10**, 1152–1163.

Chapin, C. E. & Cather, S. M. 1983. Eocene tectonics and sedimentation in the Colorado Plateau–Rocky Mountain area. Rocky Mountain Association of Geologists Guidebook 1983, 33–56.

Crowell, J. C. & Ramirez, V. R. 1979. Late Cenozoic faults in southeastern California. In: *Tectonics of the Juncture between the San Andreas Fault System and the Salton Trough, Southeastern California* (edited by Crowell, J. C. & Sylvester, A. G.). Geological Society of America Annual Meeting Guidebook, 27–39.

Diblee, T. W. 1976. The Rinconada and related faults in the southern Coast Ranges, California, and their tectonic significance. *Prof. Pap. U.S. Geol. Surv.* **981**.

Fossen, H. & Tikoff B. 1993. The deformation matrix for simultaneous simple shearing and volume change, and its application to transpression–transtension tectonics. *J. Struct. Geol.* **15**, 413–422.

Harding, T. P. 1973. Newport-Inglewood trend. Californian example of wrenching style of deformation. *Bull. Am. Ass. Petrol. Geol.* **57**, 97–116.

Harding, T. P. 1974. Petroleum traps associated with wrench faults. *Bull. Am. Ass. Petrol. Geol.* **58**, 1290–1304.

Harding, T. P. 1985. Seismic characteristics and identification of negative flower structures, positive flower structures, and positive structural inversion. *Bull. Am. Ass. Petrol. Geol.* **69**, 582–600.

Harding, T. P., Vierbuchen, R. C. & Christie-Blick, N. 1985. Structural styles, plate-tectonic settings, and hydrocarbon traps of divergent (transtensional) wrench faults. In: *Strike-slip Basin Deformation, Basin Formation and Sedimentation* (edited by Biddle, K. T. and Christie-Blick, N.). *Spec. Pubs. Soc. econ. Paleont. Miner.* **37**, 51–77.

Jamison, W. R. 1991. Kinematics of compressional fold development in convergent wrench terranes. *Tectonophysics* **190**, 209–232.

Kugler, H. G. 1959. Geological map of Trinidad (with accompanying cross-section), scale 1:100,000: Orell Fussli Arts Graphiques S.A., Zurich.

McCoss, A. M. 1986. Simple constructions for deformation in transpression/transtension zones. *J. Struct. Geol.* **8**, 715–718.

Naylor, M. A., Mandl, G. & Sijpesteijn, C. H. K. 1986. Fault geometries in basement-induced wrench faulting under different initial stress states. *J. Struct. Geol.* **8**, 737–752.

Odonne, F. & Vialon, P. 1983. Analogue models of folds above a wrench fault. *Tectonophysics* **99**, 31–46.

Richard, P., Mocquet, B. & Cobbold, P. R. 1991. Experiments on simultaneous faulting and folding above a basement wrench fault. *Tectonophysics* **188**, 133–141.

Sanderson, D. J. & Marchini, W. R. D. 1984. Transpression. *J. Struct. Geol.* **6**, 449–458.

Smith, J. G. 1965. Fundamental transcurrent faulting in northern Rocky Mountains. *Bull. Am. Ass. Petrol. Geol.* **49**, 1398–1409.

Smith, J. V. & Durney, D. W. 1992. Experimental folding of brittle structural assemblages in oblique divergence. *Tectonophysics* **216**, 235–253.

Sylvester, A. G. 1988. Strike-slip faults. *Bull. geol. Soc. Am.* **100**, 1666–1703 (Centennial Article).

Tron, V. & Brun, J.-P. 1991. Experiments on oblique rifting in brittle–ductile systems. *Tectonophysics* **188**, 71–84.

Withjack, M. O. & Jamison, W. R. 1986. Deformation produced by oblique rifting. *Tectonophysics* **126**, 99–124.

APPENDIX 1

The horizontal strain ellipse

Sanderson & Marchini (1984) define the three-dimensional deformation matrix

$$\mathbf{D} = \begin{pmatrix} 1 & \alpha^{-1}\gamma & 0 \\ 0 & \alpha^{-1} & 0 \\ 0 & 0 & \alpha \end{pmatrix}, \quad \text{(A1)}$$

where α^{-1} is the horizontal stretch, parallel to the y-axis, α is the vertical stretch, parallel to the z-axis, and γ is the horizontal shear strain, parallel to the x-axis.

The deformation in the horizontal (x-y) plane can be described by

$$\mathbf{D} = \begin{pmatrix} 1 & \alpha^{-1}\gamma \\ 0 & \alpha^{-1} \end{pmatrix}, \quad \text{(A2)}$$

and the inverse deformation is given by

$$\mathbf{D}^{-1} = \begin{pmatrix} 1 & -\gamma \\ 0 & \alpha \end{pmatrix}. \quad \text{(A3)}$$

Thus a point in the undeformed state (x, y) can be specified in terms of the deformed state (x', y'):

$$\begin{pmatrix} x \\ y \end{pmatrix} = \begin{pmatrix} 1 & -\gamma \\ 0 & \alpha \end{pmatrix} \begin{pmatrix} x' \\ y' \end{pmatrix}, \quad \text{(A4)}$$

which yields the simultaneous linear equations

$$\begin{Bmatrix} x = x' - \gamma y' \\ y = \alpha y' \end{Bmatrix}. \quad \text{(A5)}$$

Substituting equation (A5) into the equation for a unit circle in the undeformed state,

$$x^2 + y^2 = 1, \quad \text{(A6)}$$

yields the following equation for the horizontal strain ellipse in the deformed state:

$$(x' - \gamma y')^2 + \alpha^2 y'^2 = 1. \quad \text{(A7)}$$

Rewriting equation (A7) yields

$$x'^2 - 2\gamma x'y' + (\alpha^2 + \gamma^2)y'^2 = 1. \quad \text{(A8)}$$

Equation (A8) is in the form

$$c_{11}x'^2 + 2c_{12}x'y' + c_{22}y'^2 = 1, \quad \text{(A9)}$$

where

$$c_{11} = \frac{\cos^2\phi}{l_1^2} + \frac{\sin^2\phi}{l_2^2} = 1,$$

$$c_{12} = \left(\frac{1}{l_1^2} - \frac{1}{l_2^2}\right)\sin\phi\cos\phi = -\gamma,$$

$$c_{22} = \frac{\sin^2\phi}{l_1^2} + \frac{\cos^2\phi}{l_2^2} = \gamma^2 + \alpha^2, \quad \text{(A10)}$$

where l_1 is one-half the length of the major axis of the horizontal ellipse, l_2 is one-half the length of the minor axis, and ϕ is the orientation of the long axis, measured from the x-axis direction (Fig. 3). Solving these equations for ϕ, l_1 *and* l_2 yields

$$\phi = \tfrac{1}{2}\arctan\left(\frac{2\gamma}{\alpha^2 + \gamma^2 - 1}\right), \quad \text{(A11)}$$

$$l_1 = (1 - \gamma\tan\phi)^{-1/2} = S_{\text{Hmax}}, \quad \text{(A12)}$$

$$l_2 = (1 + \gamma\cot\phi)^{-1/2} = S_{\text{Hmin}}. \quad \text{(A13)}$$

These equations, given in the text, express the orientation (ϕ) of the horizontal strain ellipse and the magnitudes (S_{Hmax}, S_{Hmin}) of the horizontal principal stretches in terms of α and γ.

Solving equations (A12) and (A13) for γ yields

$$\gamma = \cot\phi\left(1 - \frac{1}{S_{\text{Hmax}}^2}\right), \quad \text{(A14)}$$

and

$$\gamma = \tan\phi\left(\frac{1}{S_{\text{Hmin}}^2} - 1\right). \quad \text{(A15)}$$

Thus γ can be determined from the orientation of the horizontal strain ellipse, γ, and the magnitude of the maximum or minimum horizontal stretch.

APPENDIX 2

The convergence factor, R

Since R is defined as the convergence component divided by the strike-slip component,

$$R = \frac{1 - \alpha^{-1}}{\alpha^{-1}\gamma} = \frac{\alpha - 1}{\gamma}. \quad \text{(A16)}$$

Solving for γ

$$\gamma = \frac{\alpha - 1}{R}. \quad \text{(A17)}$$

For divergent deformation, the width of the zone, α^{-1}, increases from 1 to infinity at the limit. Thus

$$\gamma_{\max} = -\frac{1}{R}. \quad \text{(A18)}$$

No such limit for γ exists for convergent deformation.

Solving equation (A16) for α and substituting into equation (A11) yields

$$\phi = \tfrac{1}{2}\arctan\left(\frac{2}{(R^2 + 1)\gamma + 2R}\right), \quad \text{(A19)}$$

and solving for R,

$$R = \frac{\left(\dfrac{2\gamma}{\tan 2\phi} - \gamma^2 + 1\right)^{1/2} - 1}{\gamma}. \quad \text{(A20)}$$

Now R can be determined from ϕ and γ.

For the sake of completeness, equation (A19) can be solved for γ,

$$\gamma = \frac{\dfrac{2}{\tan 2\phi} - 2R}{R^2 + 1}, \quad \text{(A21)}$$

and equation (A11) solved for α,

$$\alpha = \left(\frac{2\gamma}{\tan 2\phi} - \gamma^2 + 1\right)^{1/2}. \quad \text{(A22)}$$

APPENDIX 3

Transverse strain

From equation (7) of Sanderson & Marchini (1984), the stretch of an arbitrary horizontal line, oriented at an angle β from the x-axis (shear direction) in the deformed state, is given by

$$l = (1 + (\alpha^2 + \gamma^2 - 1)\sin^2\beta - 2\gamma\sin\beta\cos\beta)^{-1/2}. \quad \text{(A23)}$$

For a line oriented transverse to the shear zone (Fig. 3), $\beta = 90°$ and equation (A23) simplifies to

$$l_t = (\alpha^2 + \gamma^2)^{-1/2} = S_{\text{T}}, \quad \text{(A24)}$$

which is the equation given in the text.

Solving equation (A24) for α yields

$$\alpha = \left(\frac{1}{S_{\text{T}}^2} - \gamma^2\right)^{1/2}. \quad \text{(A25)}$$

Substituting equation (A25) into equation (A11) and solving for γ yields

$$\gamma = \tfrac{1}{2}\tan 2\phi\left(\frac{1}{S_{\text{T}}^2} - 1\right). \quad \text{(A26)}$$